Journal of Power Sources 239 (2013) 54–63

Contents lists available at SciVerse ScienceDirect

Journal of Power Sources

journal homepage: www.elsevier.com/locate/jpowsour

Effect of hydrogen delivery schemes on fuel cell efficiency

Jenn-Jiang Hwang*

Department of Greenergy, National University of Tainan, Tainan 700, Taiwan

HIGHLIGHTS

- Three hydrogen supply modes are discussed, i.e., flow-through, dead-end and recirculation modes.
- The flow-through mode is used to provide a benchmark for the design of the fuel cell generators.
- The anodic stoichiometric ratio ranged between 1.3 and 1.6 for step-change loading from 350 W to 700 W.
- The entrainment ratio for the recirculation mode ranged from 22% to 38%.
- The recirculation mode has higher efficiencies than the dead-end mode for stack power larger than 1.2 kW.

ARTICLE INFO

Article history:
Received 28 November 2012
Received in revised form
8 March 2013
Accepted 11 March 2013
Available online 27 March 2013

Keywords:
Proton exchange membrane fuel cell
Hydrogen delivery scheme
Recirculation mode
Dead-end mode
Flow-through mode

ABSTRACT

The objective of this paper is to investigate the effects of hydrogen supply schemes on the efficiency of a proton exchange membrane (PEM) fuel cell system. Three different hydrogen supply schemes are examined: the flow-through mode, the dead-end mode, and the recirculation mode. The electrochemical performance of the flow-through mode, determined using a commercial test station, is used to provide a benchmark for the design of the fuel cell generators operated in either the dead-end or recirculation modes. Smart control algorithms for the dead-end and recirculation hydrogen delivery modes are proposed to minimize waste from the supplied hydrogen and to avoid performance degradation due to excess water and nitrogen accumulation in the anode channels. The transient variations in flow and electrochemical characteristics of the dead-end and recirculation modes are measured and discussed in detail. Finally, a comparison of the stack and system efficiencies of the dead-end and recirculation modes is performed.

1. Introduction

The continuous rise in energy consumption and ongoing concerns about greenhouse gas (GHG) emissions has generated interest in clean and alternative energy technologies. Fuel cells, which convert the chemical energy in hydrogen to electrical energy with water and heat as the only byproducts, are widely regarded as potential candidates for alternative power systems. Among the various fuel cell types, proton exchange membrane (PEM) fuel cells are receiving the most attention because they are suitable for both vehicular and residential applications due to their high power density, low emissions, and low-temperature operation [1–4]. Their efficiency reaches as high as 60% in electrical energy conversion, along with a 90% reduction in major pollutants [5].

Advances in the design and control of reactant flows across a PEM fuel cell stack are essential to improve durability/stability in commercial applications [6,7]. In general, reactants such as hydrogen and oxygen should be excessively supplied to PEM fuel cells to prevent reactant starvation and to minimize the reactant water produced, so as to avoid the flooding that hinders reactants from reaching the reaction sites inside the cell. In addition, higher reactant flow rates result in better fuel cell performance by keeping the reactant concentration high (lower fuel utilization).

Fig. 1 shows various hydrogen supply schemes for PEM fuel cell generators. The flow-through mode, shown in Fig. 1(a), is the simplest arrangement to supply a fuel cell system with hydrogen. In this mode, the fuel stream flows through the anode compartment continuously, whereas only a portion of hydrogen in the fuel stream is consumed in the anode compartment. The excess hydrogen has the potential to minimize the liquid water and nitrogen accumulation in the anode channel. However, the flow-through mode is impractical for terrestrial applications (e.g., vehicular or residential) due to the dangers associated with un-reacted hydrogen being discharged directly to the atmosphere. This is especially important

* Tel./fax: +886 62602205.
E-mail addresses: azaijj@mail.nutn.edu.tw, azaijj@gmail.com.

0378-7753/$ – see front matter © 2013 Elsevier B.V. All rights reserved.
http://dx.doi.org/10.1016/j.jpowsour.2013.03.090

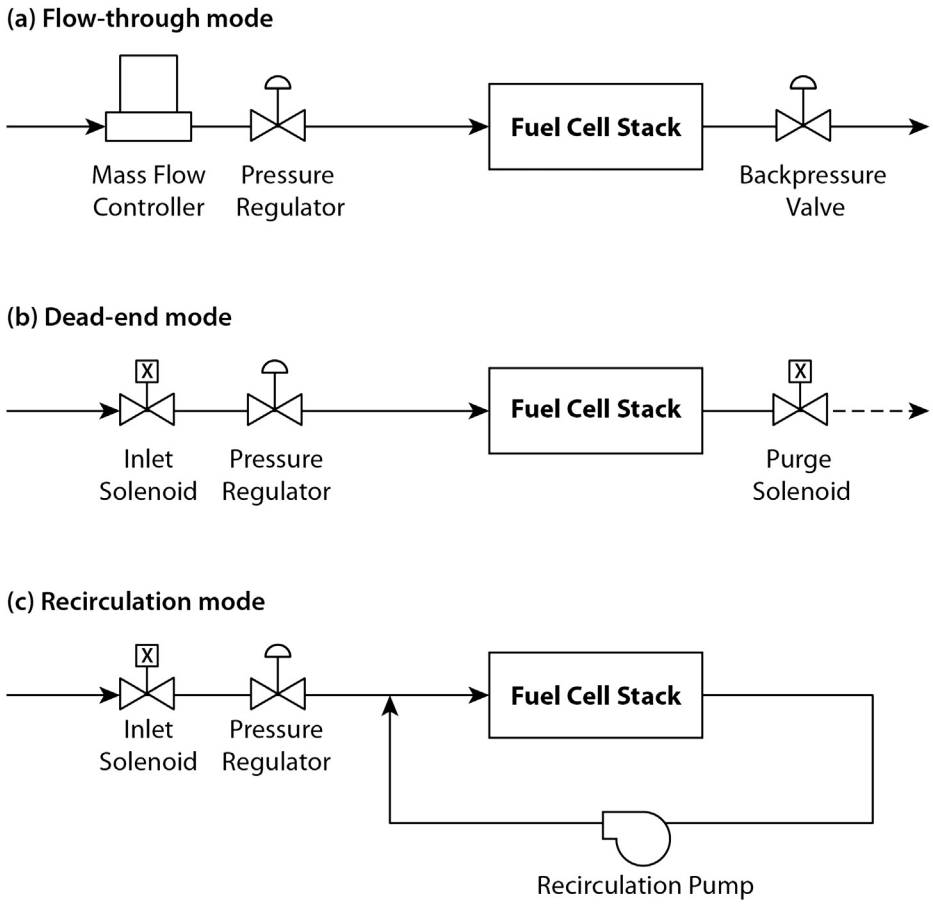

Fig. 1. Schematics of various hydrogen supply schemes.

in places with poor ventilation, such as tunnels, underground parking lots, and garages. Although there are ways to address unreacted hydrogen without generating nitrogen oxides, such as catalyst combustion, some problems may still arise. These problems include an increase in the system requirements, a potential need for expensive precious metal catalysts, and a decline in energy efficiency because the unreacted hydrogen is no longer transformed into electrical energy.

The second hydrogen delivery scheme shown in Fig. 1(b) is the dead-end mode. In this operational mode, the outlet of the anode compartment is closed, and the hydrogen is totally consumed inside the anode compartment. Any inert gases or contaminants

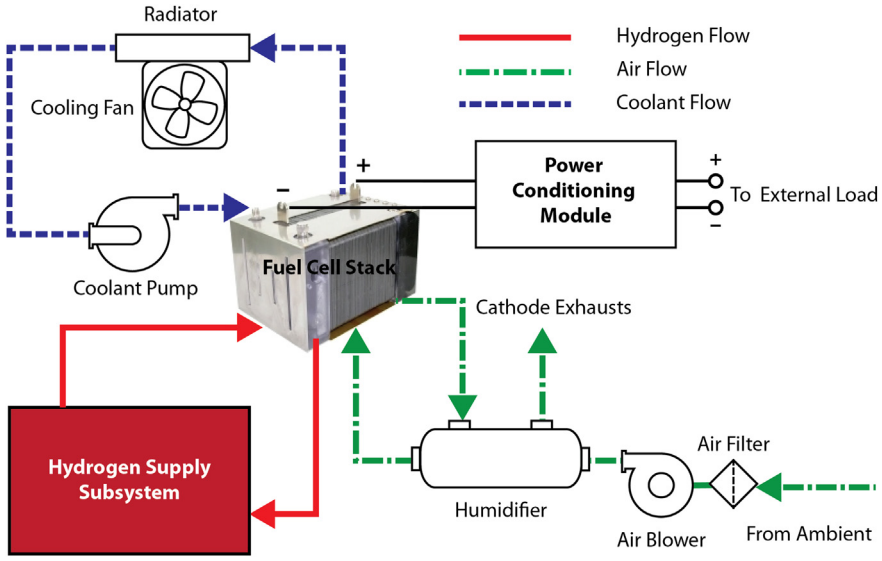

Fig. 2. Schematic drawing of the fuel cell generator.

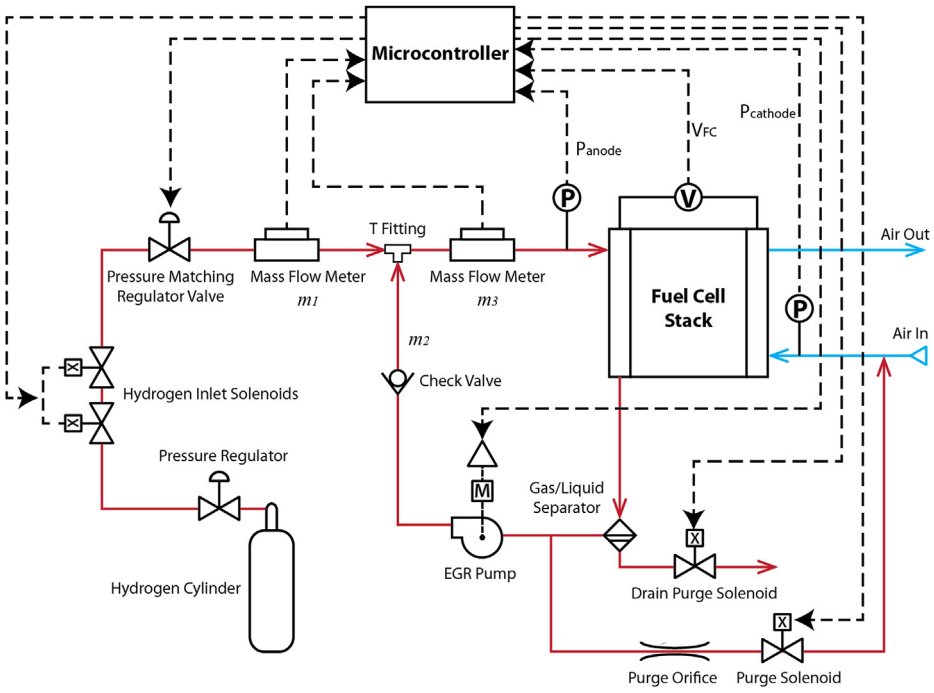

Fig. 3. Details of hydrogen recirculation mode of the fuel cell generator.

accumulate in and around the porous anodes and reduce the reaction efficiency and electrical load support capability. Therefore, this mode requires a high purity hydrogen fuel (e.g., >99.99%). In addition, water films and droplets are often found on the anode due to vapor condensation and back-diffusion of product water from the cathode. However, in this mode, hydrogen is supplied at the exact rate required by the fuel cell stack, for an anode stoichiometric ratio that is equal to or slightly less than one. Because of a lack of forced convection in the dead-end mode, the liquid water is prone to accumulate in the anodes, which eventually causes flooding and deterioration of the cell performance in the form of a decline in the voltage [8]. Therefore, purging is always employed to maintain cell performance. A purge is initiated by opening the purge valve, making the fuel cell an open-loop system. The increased flow allows the reactants to circulate through the stack, pick up liquid water and/or contaminants, and expel them through the purge lines and vents. In general, a PEM fuel cell operating in dead-end mode requires careful control of the purge frequency and duration [9–12] to ensure efficient and stable operation. Although there has been a significant amount of numerical and experimental research conducted on the time-averaged behaviors of a dead-end operated anode [6,13–19], few studies have been conducted that examine the electrochemical characteristics on a local transient level.

The third hydrogen delivery scheme, shown in Fig. 3(c), is the recirculation mode [20–22]. In this operational mode, the excess hydrogen in the exhaust from the anode is circulated back to the anode inlet by means of a recirculation pump to minimize fuel waste and avoid possible safety hazards. Although the recirculation pump consumes power generated by the fuel cell, the system efficiency increases substantially when compared to arrangements where the excess hydrogen is not re-circulated.

The objective of the present work is to experimentally study the effects of different hydrogen delivery schemes on the performance of a PEM fuel cell generator. First, the electrochemical performance for the flow-through mode, shown in Fig. 1(a), is determined using a commercial test station, which serves as the benchmark for ideal performance in the design of a PEM fuel cell generator. Then, experimental setups and control algorithms for the dead-end and recirculation modes are proposed. The goal of these designs is to approach the benchmark performance as much as possible. Transient variations in the flow and electrochemical characteristics for different hydrogen delivery schemes are examined and discussed in detail. Finally, a comparison of the stack and system efficiencies of the dead-end and recirculation modes is performed.

Table 1
Technical specifications of the fuel cell stack.

Specifications	Value
Number of cells	50
Active area	150 cm^2
Rated net output	2000 W @ 36VDC
Cut-off voltage	28 VDC
Operating temperature	40–80 °C
Anode feeding	Gaseous hydrogen, 99.99% in purity
Cathode feeding	Ambient air
Coolant	Propylene glycol/DI water mixture (50%/50%)

Table 2
Major components of the recirculation hydrogen supply subsystem.

Components	Quantity
Solenoid valve	4
Pressure regulator	2
Check valve	1
Mass flow meter	2
Gas/liquid separator	1
Pressure sensor	2
Current sensor	1
Voltage sensor	41
Purge orifice	1
EGR pump	1
Microcontroller	1

1.1. Experimental apparatus

1.1.1. Fuel cell generator

Fig. 2 schematically illustrates the fuel cell generator employed in this work. The generator consists of aPEM fuel cell stack, an airflow subsystem, a cooling subsystem, a power conditioning subsystem, and hydrogen supply subsystem. Because PEM fuel cell generators have been depicted in detail elsewhere [23–25], only the features most relevant to the work herein are briefly described below.

The fuel cell stack is made up of cells that contain two composite plates and a polymer membrane. The technical specifications of the fuel cell stack are given in Table 1. The airflow subsystem provides filtered, conditioned air to the fuel cell stack. The major components of the airflow subsystem include a cathode air filter, a cathode air blower, and a humidifier. The air filter removes volatile gas and solid contaminates from the process airstream by chemical absorption using activated carbon media and mechanical filtration. The cathode air blower (Ametek) has a variable speed motor controlled by a separate motor controller. The motor speed of the blower is a function of the DC power output of the fuel cell system. A hollow-tube membrane humidifier (Perma) transfers heat and humidity from the fuel cell stack exhaust to the inlet airstream [26]. Temperature control is performed with a pump to circulate coolant (50% propylene glycol/50% DI water) at a constant rate to remove the heat generated in the fuel cell stack. The heat is removed from the coolant through a turbofan-radiator assembly [27–31]. According to simulations [32–35], the temperature difference between a reaction site and a coolant contact boundary in a PEM fuel cell can be as much as 20 °C. Therefore, to ensure an operating temperature of approximately 80 °C in the fuel cell stack, the stack coolant inlet temperature (SCIT) is maintained at 60 °C. The power-conditioning module provides the proper interface between the stack power and the external load, as observed in Fig. 2. The major

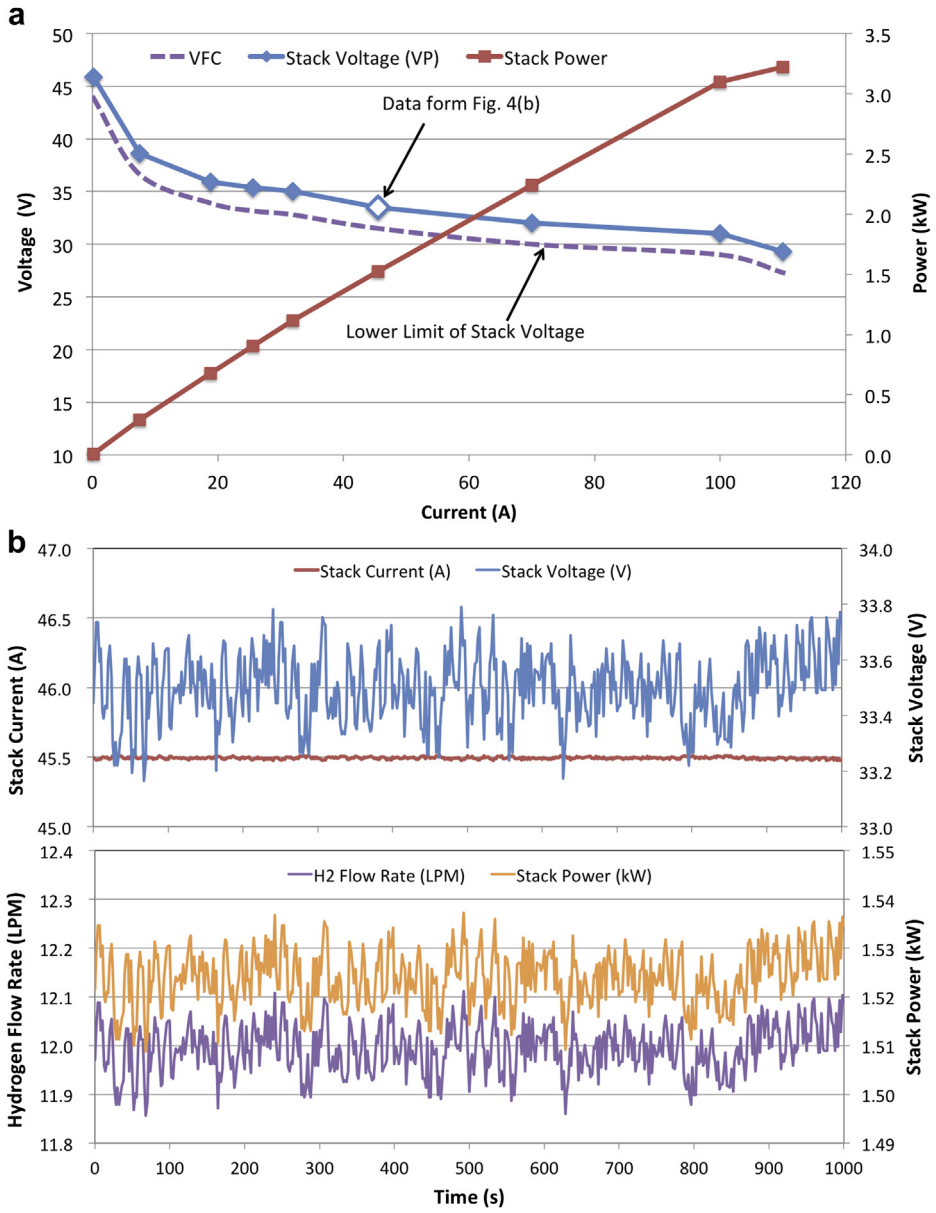

Fig. 4. Measurements for through-flow mode, (a) polarization curve, and (b) transient variation of stack voltage, stack current and hydrogen flow rate, anode stoichiometry = 1.5, cathode stoichiometry = 2.5.

components of the power-conditioning module include a bidirectional DC/DC converter, a secondary (lithium-ion) battery, a programmable electronic load, and a power controller [36]. During high power demand on the external load, the converter boosts the stack power to the DC bus, and the lithium-ion battery discharges to add extra power to the DC bus. In contrast, when the external load power demand is less than the power generated by the fuel cell stack, the converter uses the extra stack power to charge the lithium-ion battery.

1.2. Hydrogen supply scheme

Fig. 3 shows a schematic drawing of the recirculation mode hydrogen supply subsystem. The major components are listed in Table 2. The anode for the PEM fuel cell system is supplied with hydrogen from a 200 bar source, which is reduced to 4.0–7.0 bar by a directly operated pressure regulator in the hydrogen inlet pipeline. Two normally closed hydrogen inlet isolation solenoid valves allow the hydrogen to flow into the system. 24-VDC solenoid coils actuate these valves. The solenoid valves are part of the safety loop and shut off the flow of hydrogen in the event of a safety sensor trip. Additionally, these valves are plumbed in series to provide redundant protection. Furthermore, a pressure matching regulator valve is installed on the hydrogen inlet pipeline, which ensures that the pressure of the incoming hydrogen, P_{anode}, is comparable to the cathode inlet pressure, $P_{cathode}$. Such a design enhances the durability of the membrane-electrolyte assembly (MEA) by balancing the pressures across the electrolyte membrane. Two mass flow meters are installed in the hydrogen circuit before and after the T-fitting, respectively. Hydrogen that is not consumed in the anode is circulated back to the anode inlet via a hydrogen recirculation passage. An exhaust gas recirculation (EGR) pump is used to recirculate the unused hydrogen from the anode exit to the anode inlet. In contrast to the conventional arrangement used for the recirculation mode and shown in Fig. 1(c), the recirculation circuit described herein has two additional functions. First, a gas–liquid separator is installed in the recirculation passage to separate the liquid water from the unused hydrogen that prevents buildup of liquid water in the stack channels. Then, inert gases (such as nitrogen) together with limit hydrogen are exhausted into the cathode inlet through an orifice and a purge valve before reintroducing the unused hydrogen back into the main hydrogen passage. Note that the anode exhaust is burned at the cathode inlet that could help increasing the humidity of the cathode inlet stream. Due to the high-purity hydrogen (99.99%) used in the anode counterpart, there are not any harmful effects on the cell component during the experiment.

As observed in Fig. 3, a microcontroller is employed to monitor the voltages, currents, pressures, and hydrogen flow rates in the PEM fuel cell generator. These real-time data are recorded by the microcontroller and are used to assist the decision-making control algorithm. From this data, commands are sent to the microcontroller to drive actuation devices such as the solenoid valves, EGR pump, and relays that ensure proper operation of the fuel cell

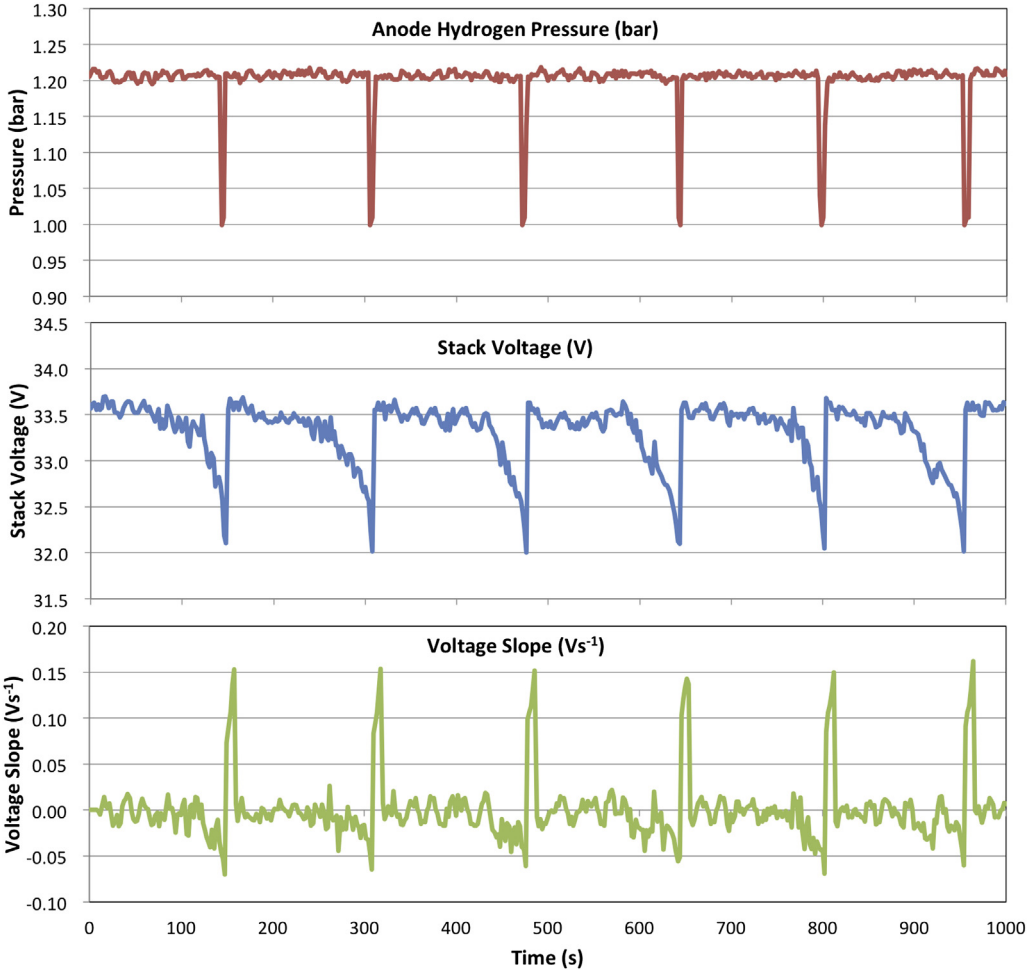

Fig. 5. Transient measurements of anode pressure, stack voltage, and voltage slope for the dead-end mode at the constant current of 45.5 A.

generator. All data and parameters collected are subsequently downloaded to a notebook through a USB communication port on the microcontroller.

2. Results and discussion

2.1. Polarization curve (flow-through mode)

Before evaluating the performance of the fuel cell generator using various hydrogen delivery schemes, it is important to understand how a fuel cell stack performs under optimal conditions. Fig. 4(a) shows the sequential polarization curves of the PEM fuel cell stack carried out on a commercial test station (Greenlight) under well-controlled operating conditions. Optimal conditions are defined as a 100% relative humidity in both the anode and cathode streams, an operating temperature maintained at 60 °C, and stoichiometric ratios for the anode and cathode streams fixed at 1.5 and 2.5, respectively. The polarization curve from the commercial test station is based on the flow-through mode for both the anode and cathode streams. Each data point on the polarization curve in Fig. 4(a) is determined by performing a 15-min hold at the desired current before proceeding to the next point. As shown in Fig. 4(b), the transient measurements show the averaged stack voltage is approximately 33.5 ± 0.3 VDC at a current of 45.5 A. Additionally, the dynamic distribution of the anodic hydrogen flow rate is proportional to the stack power, which satisfies the condition for a constant anodic stoichiometric ratio. Essentially, the flow-through mode is not applicable in a modern fuel cell generator. The polarization curve obtained herein provides the ideal electrochemical results from the fuel cell stack, which serves as a benchmark for designing the hydrogen delivery schemes in the fuel cell generators. Additionally, the electrochemical performance of a fuel cell stack is expected to decrease in a generator. For this study, the acceptable decline in the electrochemical performance of a fuel cell stack is shown by a dashed curve in Fig. 4(a) and will be discussed later.

2.2. Dead-end mode

Fig. 5 shows the transient variations in the flow and electrical characteristics of a PEM fuel cell generator with a dead-ended anode. The stack current is maintained at 45.5 A with an anode back pressure of 1.2 bar. The corresponding control routine for the dead-end mode is shown by a flowchart in Fig. 6. In the flowchart, the microcontroller first calculates the stack voltage (V_{FC}), the stack voltage rate of change ($\Delta V_{FC}/\Delta t$), and the voltage difference in the adjacent cells ($V_N - V_{N+1}$) after the fuel cell is started. Then, according to the control algorithms, the anode is purged when any of the following conditions are met.

$$V_P - V_{FC} \geq 2.0 \text{ V} \quad (1)$$

$$\Delta V_{FC}/\Delta t \leq -0.05 \text{ V s}^{-1} \quad (2)$$

$$|V_N - V_{N+1}|/V_{N+1} \geq 10\% \quad (3)$$

For the first purging criterion, the reference stack voltage, V_P, is derived from the polarization curve in Fig. 4(a) obtained for the flow-through mode using a commercial test station. The stack voltage, V_{FC}, is measured from the PEM fuel cell generator with a dead-ended anode. In general, the power delivered by the fuel cell stack in the dead-end mode should not exceed that of the polarization curve shown in Fig. 4(a) for the same stack current. In this study, a 2.0 V stack voltage drop is tolerated, which is represented by the dashed curve shown in Fig. 4(a). For stack voltage drops greater than 2.0 V, the purging process is executed.

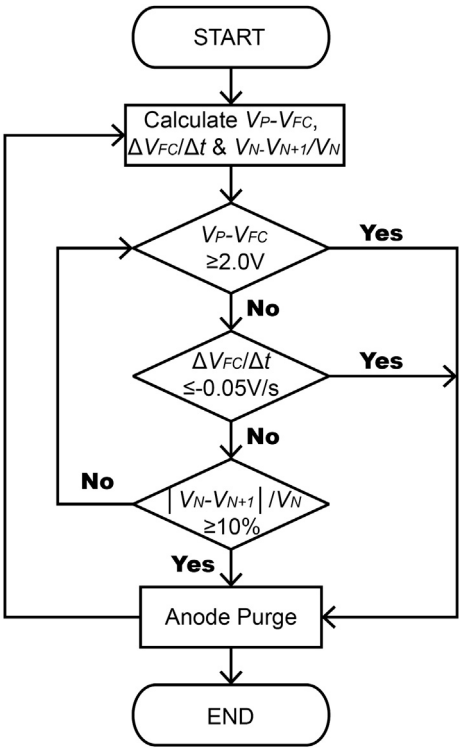

Fig. 6. Flowchart of controlling the anode purge for the dead-end mode.

For the second purging criterion, the anode outlet solenoid is purged when the stack voltage rate of change is less than -0.05 V s^{-1} for a fixed stack current. This control strategy avoids sharp declines in the stack voltage that cause deterioration in the fuel cell stack due to the strong electrodynamics in the fuel cell. Using this strategy ensures good power generation performance from the fuel cell stack and no reduction in the durability of the electrolyte membrane of each cell, which may otherwise be caused by flooding of the anode.

The third purging criterion is based on the voltage difference between adjacent cells. In an ideal case, all the cells operate with a similar and sufficient hydrogen supply, and the voltage distribution in each cell is uniform when the stack discharges (as the load increases). However, when liquid water accumulates and blocks the gas channels, the hydrogen deficiency reduces the cell voltage. When the normalization of the voltage difference between the adjacent cells is greater than 10%, it becomes necessary to recover the anode by commanding the outlet solenoid to purge the excess liquid water.

As shown in Fig. 5, the stack voltage and the stack voltage rate of change gradually decays for a constant stack current. The anode purging events are routine and occur at periods of approximately 150 s. Following an anode purge, the voltage quickly improves and will gradually decay until the next anode purge event is initiated. From Fig. 5, it is clear that the time at which the anodes are purged is decided mainly by the rate of the stack voltage drop. It is noted that the gradual decay in stack voltage observed in Fig. 5 is attributed to the accumulation of nitrogen and/or liquid water in the anode. As liquid water accumulates in the anode, the apparent area decreases and causes an increase in the apparent current density. Following a purge, the liquid water is removed, and the apparent current density returns to nominal values. Because the apparent current density is used to calculate the stack voltage, the estimation of the stack voltage is sensitive to the degree of flooding in the anode. After the liquid water is removed, the stack voltage returns to approximately the same value.

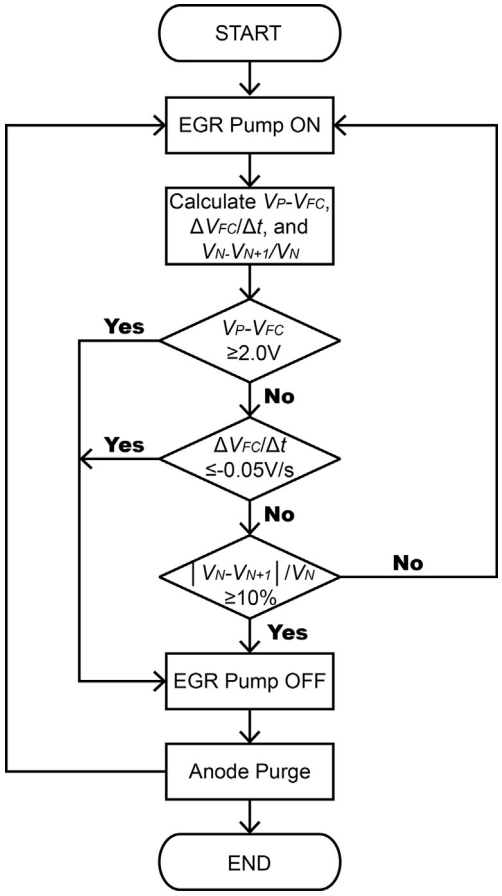

Fig. 7. Flowchart of the anode hydrogen delivery for the recirculation mode.

2.3. Recirculation mode

Fig. 7 shows a flowchart of the recirculation-mode hydrogen delivery scheme. According to the flowchart, the microcontroller commands the EGR pump to turn off after one of the three criteria described in Eqs. (1)–(3) is met. After this occurs, an anode purge is executed. The EGR pump operates constantly if no purges are required.

In addition to the constant-load measurement in determining the steady-state fuel cell efficiency, the experiments of step-change in loading are conducted to examine the effect of load dynamics on the power and hydrogen flow characteristics for the recirculation mode. Fig. 8 shows the transient variations in the stack current and the stack voltage under a rectangular-wave load (shown by the green dashed lines). At system startup, the stack voltage increases sharply to the open circuit voltage (OCV) at about $t = 25$ s. Then, the stack current/stack voltage steps up/down as the load increases. During the periodic-load period, the stack-current distribution is proportional to the external load, and the stack voltage stays in a relatively narrow range of 32–36 VDC.

Fig. 9 shows the hydrogen flow characteristics in the anodic circuit for the recirculation mode under a rectangular-wave load. Fig. 9(a) gives the transient variation in the hydrogen flow rates in the anodic circuit, including the source hydrogen flow rate (*m1*), the hydrogen recirculation flow rate (*m2*), and the hydrogen flow rate through the stack anode (*m3*). Note that the source hydrogen flow rate, *m1*, represents the hydrogen utilization in the fuel cell stack. Therefore, the transient distribution of *m1* is largely similar to that of the external load, that is, namely, the hydrogen supply to the fuel cell generator depends on the power demanded from the external load.

From the hydrogen flow rate measurements, the anode stoichiometric (*m3/m1*) and entrainment ratios (*m2/m3*) are determined and displayed in Fig. 9(b). The anode stoichiometric ratio varies from 1.3 to 1.6 during the periodic rectangular-wave loading. The general tendency is that a lower external load requires a higher anode stoichiometry. The entrainment ratio ranges from 22% to 38% during the periodic rectangular-wave loading.

Fig. 10 compares the hydrogen flow rate through the stack anode for the flow-through and recirculation modes under the rectangular-wave loading. Note that to avoid deterioration in the fuel cell stack caused by anode starvation, the feed hydrogen in the stack anode should not be totally consumed. In this work, the flow-through mode anode stoichiometric ratio is designed to be 1.5. This means that about one-third of the hydrogen is unused and exhausts to the anode outlet. For the recirculation mode, the feed hydrogen rate *m1* is almost the same as the consumption rate, and the anode stoichiometric ratio is maintained between 1.3 and 1.6 by re-circulating the

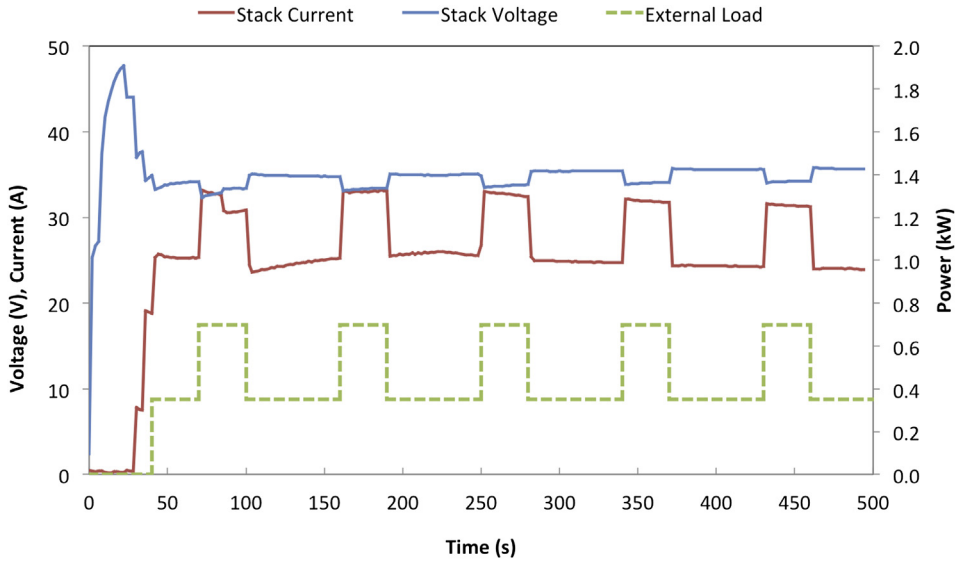

Fig. 8. Transient variations of voltage and current for the rectangular-wave load profile under recirculation mode.

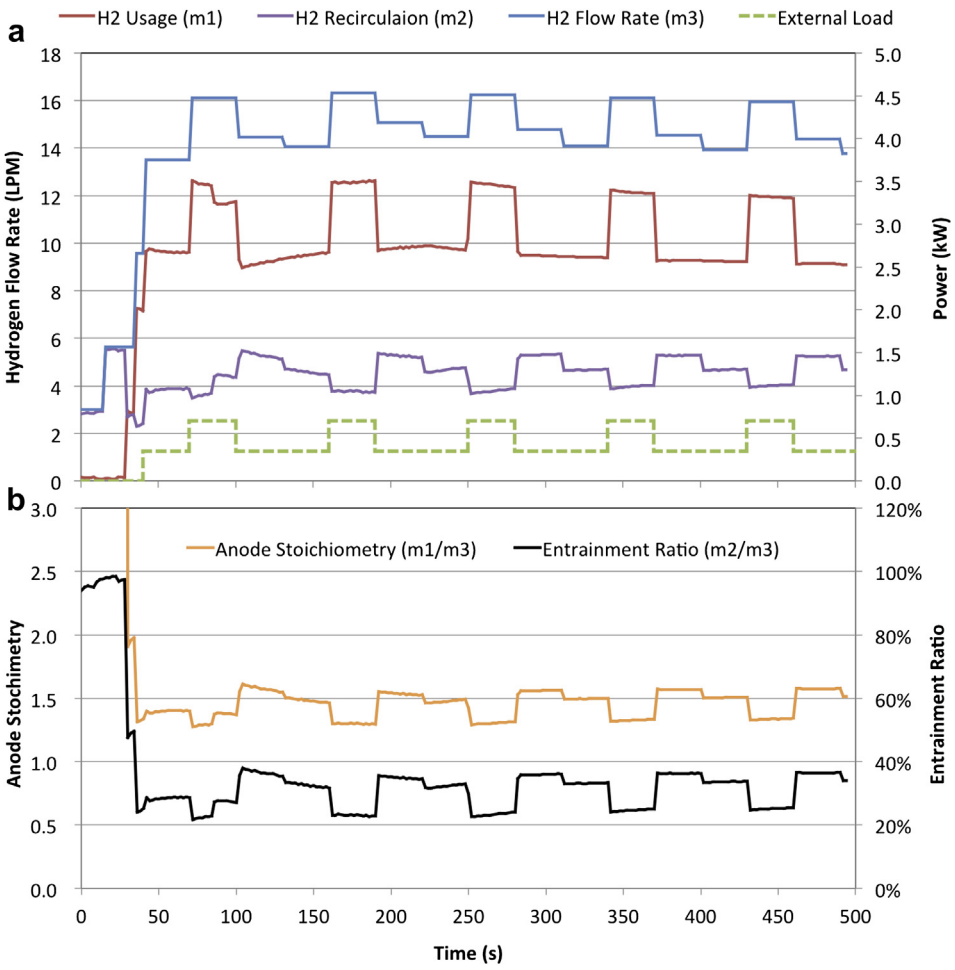

Fig. 9. Hydrogen flow characteristics for the recirculation mode, (a) hydrogen flow rates (b) entrainment ratio and stoichiometric ratio.

unused hydrogen, *m2*. The recirculation mode provides the necessary forced convection in the anode channels without any hydrogen exhausting to the anode outlet (except for the conditional purges), which is favorable from an efficiency standpoint.

2.4. Efficiency analysis

Two types of fuel cell efficiencies are discussed in this work, stack efficiency and system efficiency. Stack efficiency is defined as

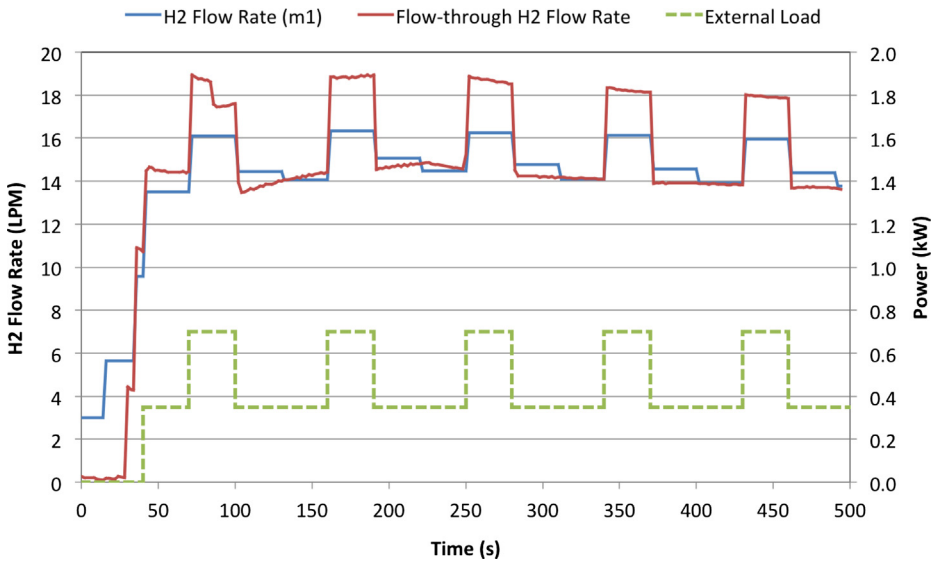

Fig. 10. Comparison of the hydrogen flow rate across the fuel cell stack between and the recirculation mode and the flow through mode.

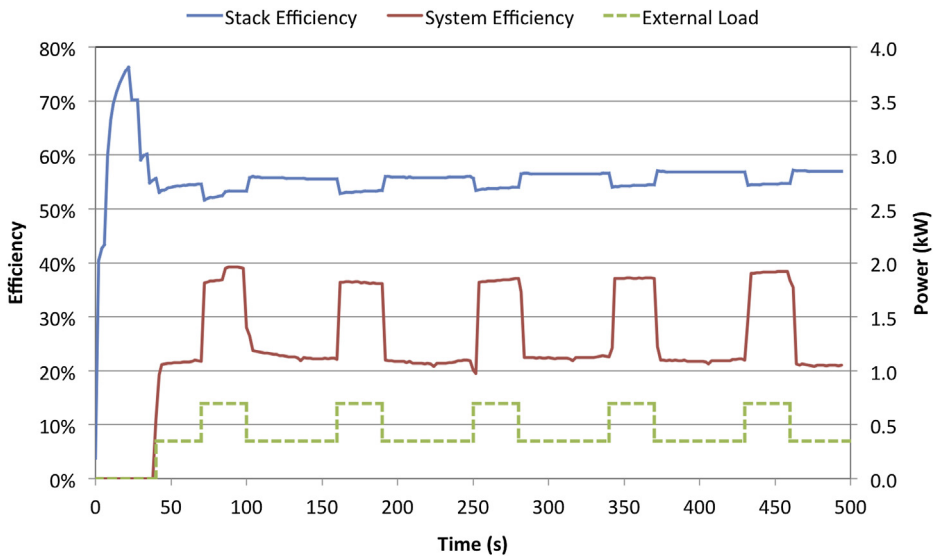

Fig. 11. Dynamics of the stack efficiency and the system efficiency for the recirculation mode.

the ratio of the stack gross power (P_{stack}) to the hydrogen power consumption (P_{H_2}) in the anode:

$$\varepsilon_{stack} = P_{stack}/P_{H_2} = I_{stack} \times V_{stack}/M_{H_2} \times m_{H_2} \times \Delta h \quad (4)$$

where m_{H_2} is the mass flow rate of the hydrogen, M_{H_2} is the molar weight of hydrogen, and Δh Is the enthalpy of hydrogen. The gross power from the fuel cell stack is derived from the measured stack current (I_{stack}) and stack voltage (V_{stack}). The hydrogen mass flow rate in Eq. (4) is read directly from the mass flow meter.

Because a PEM fuel cell system consists of some balance-of-plants (BOPs), such as radiator fans, coolant pumps, and air blowers [37], part of the stack power is used to drive these BOPs to keep the system running. In addition, the power conversion mechanism, which uses DC/DC converters to regulate the voltage of the fuel cell when the output current changes results in some power loss. The net power transmitted to the external load is defined the gross stack power with all the auxiliaries subtracted off. Therefore, the system efficiency is defined as the ratio of the net power transmitted to the external load P_{load} to the hydrogen power consumption:

$$\varepsilon_{system} = P_{load}/P_{H_2} = I_{load} \times V_{load}/M_{H_2} \times m_{H_2} \times \Delta h \quad (5)$$

The net power transmitted to the external load, P_{load}, is determined from the voltage across the external load (V_{load}) and the current in the circuit (I_{load}).

Fig. 11 shows the transient variations in the recirculation mode stack and system efficiencies of the fuel cell generator under the rectangular-wave loading. The blue curve represents the stack efficiency, and the red curve represents the system efficiency. Under the periodic rectangular-wave loading, the system efficiency varies between 22% and 38%, whereas the stack efficiency remains constant at approximately 54 ± 2%.

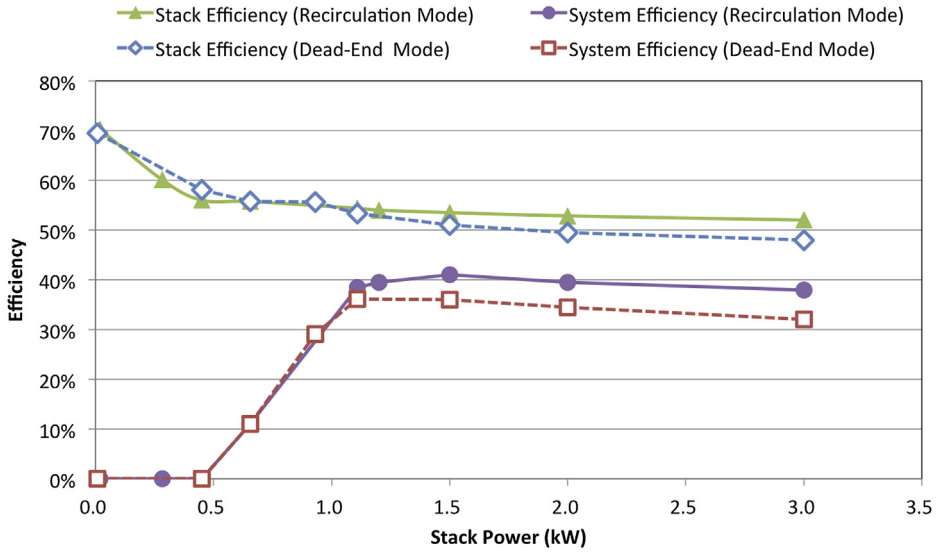

Fig. 12. Comparison of stack and system efficiency between the recirculation mode and the dead end mode under various stack powers.

Fig. 12 displays the averaged stack and system efficiencies as a function of the stack gross power. Both efficiencies are strongly dependent on the gross power delivered by the fuel cell stack. In general, the stack efficiency decreases for low stack power conditions ($P_{stack} < 1.0$ kW) but does not greatly change for higher powers ($P_{stack} > 1.5$ kW). The system efficiency is zero for $P_{stack} < 0.45$ kW, as all the stack power is used to drive the BOPs. At stack powers of $P_{stack} < 0.45$ kW, the system efficiency increases to greater than 40% at powers of roughly $P_{stack} < 1.5$ kW. At greater powers, the system efficiency declines slightly.

Both the system and stack efficiencies have very similar efficiencies at stack powers of $P_{stack} < 1.2$ kW for both of the two hydrogen delivery schemes. By contrast, as the stack power becomes greater than 1.2 kW, the recirculation mode has higher system and stack efficiencies than the dead-end mode. This may be because the purging frequency is significantly higher for the dead-end mode. For the dead-end mode, the hydrogen mass and liquid water can be visually detected leaving the anode and impacting the system efficiency.

3. Conclusions

In this work, the effects of different hydrogen supply schemes on the efficiency of a PEM fuel cell system has been studied experimentally. The electrochemical performance of the flow-through mode was determined using a commercial test station that served as the benchmark for the fuel cell generator designs using the various hydrogen delivery schemes. Self-designed experimental setups and smart control strategies were used to examine the performance of the fuel cell generator in both dead-end and recirculation modes. Transient measurements of the flow and electrochemical characteristics revealed that conditional anode purging stabilizes the stack voltage for constant stack currents in the dead-end mode. In the recirculation mode, the anodic stoichiometric ratio ranged between 1.3 and 1.6 under periodic step-change loading from 350 W to 700 W, which is comparable to that of the flow-through mode operated using the commercial test station. Further results showed that the recirculation mode entrainment ratio ranged from 22% to 38%, which is reversely related to the external load. The system efficiency was found to be between 22% and 38%, whereas the stack efficiency remained constant at approximately 54 ± 2% for the recirculation mode. Furthermore, for stack powers less than 1.2 kW, both the dead-end and recirculation modes have roughly the same stack and system efficiencies. By contrast, when the stack power is greater than 1.2 kW, the recirculation mode has higher system and stack efficiencies than the dead-end mode.

Acknowledgments

The author professor Jenn-Jiang Hwang would like to thank the National Science Council of Taiwan, for financially supporting this research under contract no. NSC 98-2221-E-024-015-MY2.

References

[1] Fuel Cell Handbook, seventh ed., EG&G Technical Services, Inc, 2004.
[2] M. Granovskii, I. Dincer, M.A. Rosen, J. Power Sources 157 (2006) 411–421.
[3] J.J. Hwang, W.R. Chang, Int. J. Hydrogen Energy 35 (2011) 11946–11956.
[4] G. Gigliucci, L. Petruzzi, E. Cerelli, A. Garzisi, A. La Mendola, J. Power Sources 131 (2004) 62–68.
[5] J.J. Hwang, Renewable Sustainable Energy Rev. 16 (2012) 3803–3815.
[6] P. Mocoteguy, F. Druart, Y. Bultel, S. Besse, A. Rakotodrainibe, J. Power Sources 167 (2007) 349–357.
[7] W.R. Chang, J.J. Hwang, J. Power Sources 166 (2007) 149–154.
[8] J.J. Hwang, W.R. Chang, R.G. Pen, P.Y. Chen, A. Su, Int. J. Hydrogen Energy 33 (2008) 5718–5727.
[9] J.W. Choi, Y.S. Hwang, J.H. Seo, D.H. Lee, S.W. Cha, M.S. Kim, Int. J. Hydrogen Energy 35 (2010) 3698–3711.
[10] N. Bussayajarn, H. Ming, K.K. Hoong, W.Y.M. Stephen, C.S. Hwa, Int. J. Hydrogen Energy 34 (2009) 7761–7767.
[11] W.H. Zhu, R.U. Payne, B.J. Tatarchuk, J. Power Sources 156 (2006) 512–519.
[12] R.K. Ahluwalia, X. Wang, J. Power Sources 171 (2007) 63–71.
[13] S. Hikita, F. Nakatani, K. Yamane, Y. Takagi, JSAE Rev. 23 (2002) 177–182.
[14] L. Dumercy, M.C. Pera, R. Glises, D. Hisel, S. Hamandi, F. Badin, Fuel Cells 4 (2004) 352–357.
[15] O. Himanen, T. Hottinen, S. Tuurala, Electrochem. Commun. 9 (2007) 891–894.
[16] W.R. Baumgartner, P. Parz, S.D. Fraser, E. Wallnofer, V. Hacker, J. Power Sources 182 (2008) 413–421.
[17] J.B. Siegel, D.A. McKay, A.G. Stefanopoulou, J. Electrochem. Soc. 155 (2008) B1168–B1178.
[18] Y. Lee, B. Kim, Y. Kim, Int. J. Hydrogen Energy 34 (2009) 7768–7779.
[19] A.P. Sasmito, A.S. Mujumdar, Int. J. Hydrogen Energy 36 (2011) 10917–10933.
[20] Y. Sone, M. Ueno, S. Kuwajima, J. Power Sources 137 (2004) 269–276.
[21] Y. Sone, M. Ueno, H. Naito, S. Kuwajima, J. Power Sources 157 (2006) 886–892.
[22] C. Bao, M. Ouyang, B. Yi, Int. J. Hydrogen Energy 31 (2006) 1879–1896.
[23] J.J. Hwang, D.Y. Wang, N.C. Shih, D.Y. Lai, C.K. Chen, J. Power Sources 133 (2004) 223–228.
[24] J.J. Hwang, D.Y. Wang, N.C. Shih, J. Power Sources 141 (2005) 108–115.
[25] J.J. Hwang, W.R. Chang, J. Power Sources 207 (2012) 111–119.
[26] J.J. Hwang, J. Power Sources 219 (2012) 317–324.
[27] J.J. Hwang, C.S. Cheng, J. Heat Transfer 121 (1999) 683–690.
[28] J.J. Hwang, T.M. Liou, J. Heat Transfer 116 (1994) 912–920.
[29] J.J. Hwang, D.Y. Lai, Int. J Heat Mass Transfer 8–9 (1998) 979–991.
[30] T.M. Liou, J.J. Hwang, S.H. Chen, J. Thermophys. Heat Transfer 6 (1992) 513–521.
[31] J.J. Hwang, G.J. Hwang, R.H. Yeh, C.H. Chao, J. Heat Transfer 124 (2002) 120–129.
[32] J.J. Hwang, J. Electrochem. Soc. 153 (2006) A216–A224.
[33] J.J. Hwang, P.Y. Chen, Int. J. Heat Mass Transfer 49 (2006) 2315–2327.
[34] J.J. Hwang, C.H. Chao, Int. J. Hydrogen Energy 32 (2007) 405–414.
[35] J.J. Hwang, J. Power Sources 164 (2007) 174–181.
[36] J.J. Hwang, W.R. Chang, J. Chin. Soc. Mech. Eng. 32 (2011) 181–187.
[37] J.J. Hwang, J. Power Sources 223 (2013) 325–335.